

Material gain concentration quenching in organic dye-doped polymer thin films

FLORIAN VOGELBACHER,^{1,2,*} XUE ZHOU,³ JINHUA HUANG,³ MINGZHU LI,³ KE-JIAN JIANG,³ YANLIN SONG,³ KARL UNTERRAINER,² AND RAINER HAINBERGER¹

¹AIT Austrian Institute of Technology GmbH, Center for Health & Bioresources, Giefinggasse 4, 1210 Vienna, Austria

²TU Wien, Photonics Institute, Gusshausstr. 27-29, 1040 Vienna, Austria

³Institute of Chemistry, Chinese Academy of Science, Beijing 100190, P.R. China

*florian.vogelbacher.fl@ait.ac.at

Abstract: The optimization of material gain in optically pumped dye-doped polymer thin films is an important task in the development of organic solid-state lasers. In this work, we present a theoretical model that accommodates the influence of concentration quenching on material gain and employ it to study the novel dye molecule 2-(4-(bis(4-(*tert*-butyl)phenyl)amino)benzylidene)-malononitrile (PMN) and the well-established dye molecule 4-(dicyanomethylene)-2-methyl-6-(4-dimethylaminostyryl)-4H-pyran (DCM) embedded in poly(methyl methacrylate) (PMMA). Polycarbonate was tested as an alternative host material for PMN. The material gain in these dye-doped polymer thin films was determined by the variable stripe length method. The inclusion of concentration quenching in the material gain expression is able to significantly reduce the overestimation of the gain efficiency inherent to a linear model.

© 2024 Optical Society of America under the terms of the [OSA Open Access Publishing Agreement](#)

1. Introduction

Photonic technology based on polymer materials provides a versatile platform for applications in data- & telecommunication, sensing, and medical diagnostics, achievable by a broad range of material properties, flexibility in fabrication, and low cost [1–4]. Suitable optical and optoelectronic characteristics enabled the development of organic solar cells [5, 6] and highly efficient light sources, such as organic solid-state lasers [7] and light emitting diodes (OLEDs) [8–10]. In contrast to OLEDs, the feasibility of direct electrical pumping of organic solid-state lasers and continuous wave operation are still an open research topic. Therefore, organic solid-state lasers are driven by pulsed optical excitation [7, 11, 12]. Different optical pump sources such as inorganic solid-state lasers, semiconductor laser diodes [13–15], or light-emitting diodes (LEDs) [13, 16] have been successfully employed [17]. Due to their compact size and comparatively low cost semiconductor laser diodes and LEDs are particularly promising pump sources for applications in organic solid-state lasers in hand-held and point-of-care devices. Even though the lifetime of organic dyes under strong optical excitation is limited due to photobleaching [18–20], their use in low cost sensing applications and single-use devices might be favorable compared to more expensive semiconductor devices. The possibility to locally deposit the dye-doped polymer material on the substrate via ink-jet printing can decrease fabrication costs even further and adds additional design flexibility [21, 22]. Compatibility to CMOS fabrication processes enables the co-integration of organic polymer based technology with microelectronics.

Small molecular dyes embedded in transparent host materials are, in general, a popular class of organic gain materials for organic dye lasers due to their wide spectral emission properties ranging from the near ultra violet to near infrared wavelength region. Early works investigated the influence of dye concentration, excitation intensity, and pulse width on lasing properties of liquid dye lasers [23, 24]. However, for thin film polymer solid-state lasers concentration

dependent lasing properties have not been widely reported despite the strong influence of the doping level and the host matrix [25–27]. In particular, the evaluation of the material gain is a prerequisite for the development and proper choice of dye molecules as well as the selection of suitable host polymers, as concentration quenching ultimately limits attainable modal gain.

In this work, we present a model for material gain concentration quenching. We tested it against gain properties of the novel electron donor-electron acceptor dye molecule 2-(4-(bis(4-*tert*-butyl)phenyl)amino)benzylidene)malononitrile (PMN), which was designed for improved intramolecular charge transfer and broad spectral absorption in the visible region, and the commercially available dye molecule 4-(dicyanomethylene)-2-methyl-6-(4-dimethylaminostyryl)-4H-pyran (DCM), which represents a good reference due to its widespread use as a gain material. The influence of the host polymer matrix on the quenching was investigated by embedding PMN in poly(methyl methacrylate) (PMMA) and polycarbonate (PC). The results were compared against the proposed quenching model. Gain properties of dye-doped PC thin films have not yet been published widely, despite its broad use in light guiding, optics, optical data storage and light sources as an highly transparent plastic [32]. The higher refractive index of PC compared to PMMA is an interesting material property for integrated photonic designs. The modal gain of the dye-doped polymer thin films was determined by the variable stripe length (VSL) method [28–31]. Optical excitation of the gain material was performed by a high power 450 nm blue laser diode enabling a material characterization at the exact wavelength, optical intensity, and temporal pulse shape of the envisaged light source.

2. Materials and method

2.1. Organic dyes

For the synthesis of the novel dye, freshly distilled POCl_3 (28.4 mL, 12.5 eq) was added dropwise to dimethylformamid (DMF) (21.7 mL, 12 eq) under an atmosphere of N_2 at 0°C in ice bath, and then it was stirred for 1 h. *N,N*-Di(4-*tert*-butylphenyl)aniline (4.3 g, 12 mmol) was added to the above solution, and the resulting mixture was stirred for 4 h at 0°C . Then, the mixture was poured into a beaker containing ice-cubes, and basified with 4 M NaOH. The solid was filtered and extracted with ethylacetate (EA)-brine. After evaporating the organic solvent, the crude product was purified by column chromatography on silica using a mixture of EA-hexane (1:6, v/v), to give 4.1 g of a yellow solid [35]. Under an atmosphere of dry nitrogen, 4-[Bis[4-(1,1-dimethylethyl)phenyl]amino]benzaldehyde (2 g, 5 mmol) and malononitrile (0.6608 g, 10 mmol), dissolved in toluene (50 mL), were refluxed 24 h using trace piperidine as the catalyst. Then, the reaction mixture was cooled to room temperature and the solvent was removed under reduced pressure. The resultant residue was purified by silica gel column chromatography using ethyl acetate and hexane (1:8, v/v) as eluents to afford the product as an orange-red solid (1.8 g, 83%), 2-(4-(bis(4-*tert*-butyl)phenyl)amino)benzylidene)malononitrile (PMN).

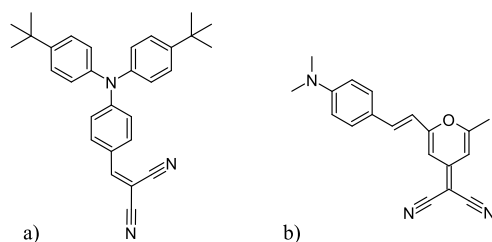


Fig. 1. Molecular structure of (a) 2-(4-(bis(4-*tert*-butyl)phenyl)amino)benzylidene)malononitrile (PMN), and (b) 4-(dicyanomethylene)-2-methyl-6-(4-dimethylaminostyryl)-4H-pyran (DCM).

Figure 1(a) shows the molecular structure of the resulting dye. The tert-butyl decorated triphenylamine functions as donor and the cyanogroups act as acceptor. The bulky tert-butyl groups also improve the solubility, impede dye aggregation, and reduce concentration quenching. PMN shares a similar design to *fvin*, an organic dye presented in [36, 37]. The commercially available benchmarking dye DCM, depicted in Fig. 1(b), was obtained from Sigma-Aldrich and was used without additional processing. Absorbance and fluorescence emission spectra of dye-doped polymer thin films on microscope cover slides were obtained by fluorescence spectroscopy (PerkinElmer, EnSpire). The excitation wavelength for the emission measurements was set to 450 nm to be compatible with the operation wavelength of the pump laser diode used in the gain measurements later on.

2.2. Thin film preparation

Optical quality PMMA (Polycasa, Acryl G77, refractive index $n_{\text{PMMA}} = 1.492$) granulate was dissolved in anisole (Sigma-Aldrich, $\geq 99\%$) under magnetic stirring at 30°C , whereas 1,4-dioxane (Roth, $\geq 99.5\%$) was used to prepare the PC (Covestro AG, Makrolon LED2245, refractive index $n_{\text{PC}} = 1.584$) solution. The corresponding dye was added to the solution after the polymer was completely dissolved. Different dye concentrations ranging from 0.5 wt.% to 5.0 wt.% have been obtained by mixing stock solutions. Since the solubility of DCM in 1,4-dioxane was limited, the material system DCM in PC was not deployed. The mass fractions of the dissolved polymers in solution were set to 10 wt.% for PC and 15 wt.% for PMMA, respectively, to achieve suitable viscosities for spin coating. Microscope cover slides (Menzel, $25\text{ mm} \times 25\text{ mm}$) and silicon samples ($20\text{ mm} \times 20\text{ mm}$) with a $2\text{ }\mu\text{m}$ silicon dioxide ($n_{\text{SiO}_2} = 1.46$) layer were cleaned with an alkaline detergent solution (Hellma, Hellmanex) in an ultrasonic bath, thoroughly rinsed with deionized water, ultrasonically cleaned in acetone and isopropanol, and blow dried using nitrogen. Prior to spin coating, all substrates were dehydrated at 200°C for 5 min on a hot plate. The higher refractive indices of the polymers compared to the silicon dioxide film on the silicon sample enable waveguiding for VSL measurements. PMMA thin films were prepared by spin coating in an open bowl configuration, resulting in thin film thickness of $800 \pm 50\text{ nm}$. For improved thin film quality of the PC resist, spin coating was conducted in a small volume closed bowl configuration flushed with nitrogen. A two step process was used to improve adhesion of the PC film to the substrate: In a first run, a 15 nm thin non-doped PC layer was spin coated on the substrate and placed onto a hot-plate at 200°C for 1 min, heating the samples above the polymer glass temperature. In a second step, the dye doped PC thin film was deposited onto the substrate, resulting in a total thin film thickness of $650 \pm 50\text{ nm}$. A baking step, common for both polymer types, at 110°C for 1 min on a hot plate removed residual solvent without thermal bleaching the dye. Thin film thickness was determined through evaluation of the step height of locally removed polymer by stylus profilometry (KLA-Tencor, Alpha-Step IQ). The silicon samples for gain measurements were cleaved to obtain a sharp edge and to enable a measurement at a well defined thin film thickness at the center of the sample.

2.3. Optical setup

Short current pulses at a repetition rate of 3 Hz were generated by a pulse driver (PicoLAS, LDP-V 50-100) to drive a TO-can high power multimode 450 nm laser diode (Nichia NDB7K75), reaching an electric current of up to 40 A. Figure 2 shows the optical setup to create a high intensity pump spot on the sample for VSL measurements. An aspheric lens L1 collimated the strongly diverging laser diode beam. The combination of a half-wave plate and a linear polarizer allowed rotating the input beam polarization and attenuating the pump intensity without changing the laser diode drive current. A change in laser diode drive current would influence the optical pump pulse shape and thereby the gain measurements [16]. Truncation of the pump beam for

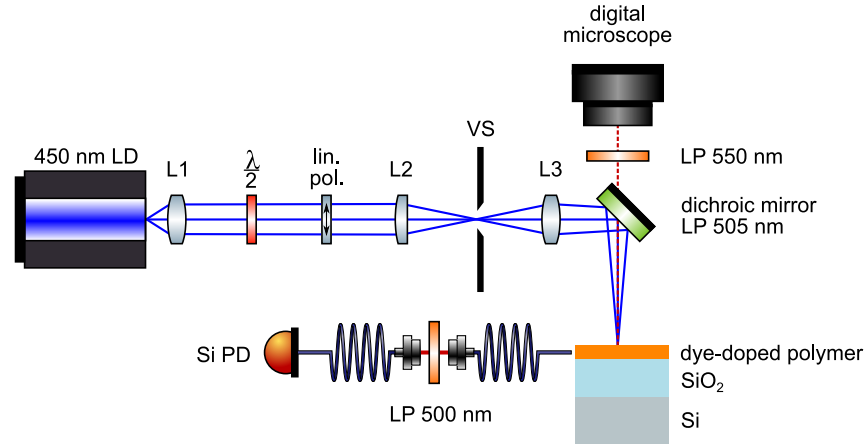


Fig. 2. Optical setup to generate a high intensity pump stripe on the sample surface. The intermediate image is used to add a variable slit (VS) minimizing Fresnel diffraction for variable stripe length (VSL) gain measurements. In this VSL setup no cylindrical lens is needed because the emission characteristics of the high power 450 nm multimode laser diode directly results in a narrow pump stripe. The light emitted from the sample edge is coupled into a multimode fiber and detected by a silicon photodiode (Si PD). A 500 nm long pass (LP) filter suppresses spurious pump light coupled into the fiber. Alignment of the pump stripe to the sample edge and fiber is achieved by inspection through a 550 nm LP filter.

VSL measurements leads to Fresnel diffraction effects on the sample surface, which potentially degrade the quality of the gain measurements [29]. In our setup, we minimized these diffraction effects of the pump beam by placing a variable slit (VS) at an intermediate image created by lens L2. The slit width was adjusted by a manual micrometer drive. In contrast to other optical setups, where a cylindrical lens was used to form a thin stripe [31, 38], the large aspect ratio of the pump spot originated directly from the laser diode emission characteristics. The slit was imaged, deflected by a dichroic mirror, onto the sample surface by lens L3 creating a $400\text{ }\mu\text{m}$ by $20\text{ }\mu\text{m}$ stripe. Intensities of approximately 150 kW cm^{-2} for 35 ns pulses were reached. A digital microscope was used to align the optical setup with the sample. Back reflected pump light from the sample surface, which spuriously passed the dichroic mirror, was blocked by a 550 nm long pass filter. A multimode fiber (0.10 NA, $10\text{ }\mu\text{m}$ core diameter) attached to a three axis flexure stage guided the light collected at the sample edge to a silicon photodiode (Si PD) connected to a lock-in amplifier. A 500 nm long pass filter mounted in a free space fiber-to-fiber bench suppressed pump light scattered and coupled into the fiber. The polarization of the pump light was set perpendicular to the long axis of the pump spot, resulting in a dominantly transverse electric (TE) amplified spontaneous emission into the stripe [39].

The resulting temporal and spatial shapes of the optical pump setup are shown in Figs. 3(a) and 3(b), respectively. The temporal behaviour was measured by a 1 GHz silicon photodiode connected to an oscilloscope with 1 GHz bandwidth. The full width at half maximum (FWHM) of the optical pulse was 35 ns at a peak driving current of 38 A. The spatial pump intensity variation was measured to be less than 20% along the pump stripe and diffraction effects of the variable slit were efficiently suppressed. Side lobes of -6 dB compared to the main pump stripe intensity originating from the laser diode emission characteristics occurred symmetrically to the main pump stripe. These weak side lobes are not expected to detrimentally influence the gain measurements.

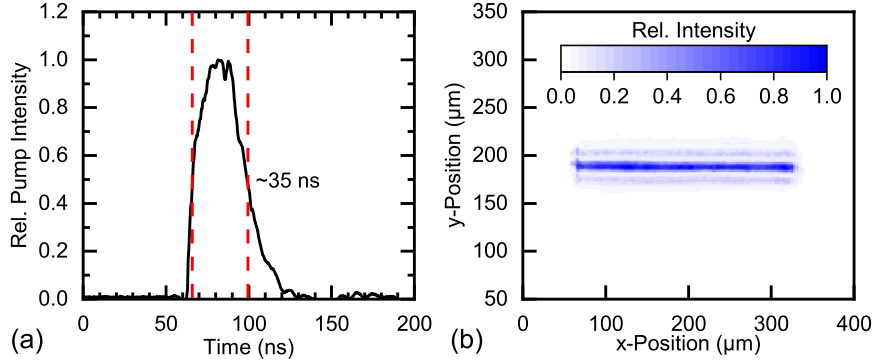


Fig. 3. (a) Temporal pump power characteristics of the laser diode driven by a pulsed current source. (b) Spatial intensity profile of the pump stripe. The optical setup suppresses Fresnel diffraction resulting in a sharp truncation of the pump stripe. Weak side lobes occur due to the emission characteristics of the LD pump source.

2.4. Variable stripe length method

Amplified spontaneous emission (ASE) measurements in a variable stripe length configuration are commonly employed to determine the modal gain g_{mod} of polymer thin film gain media, which can subsequently be used to extract the material gain. To account for geometrical effects of the narrow pump stripe and the influence of the light collecting fiber, but before intensity dependent saturation effects arise, an expression for the amplification of spontaneous emission is presented in the following.

Optical excitation of the embedded dye molecules leads to a local fluorescence emission density $I'_{\text{fl}}(x, z)$. In absence of amplification, the contribution to the light collected by the fiber at a given z -position can be written as the integral across the pump stripe resulting in an effective fluorescence density

$$I'_{\text{fl,eff}}(z) = \int_{-W/2}^{W/2} I'_{\text{fl}}(x, z) \frac{\Omega(x, z)}{2\pi} \gamma(x, z) dx, \quad (1)$$

with the pump stripe width W , the solid angle $\Omega(x, z)$ and the fiber coupling efficiency $\gamma(x, z)$. The solid angle depicted in Fig. 4 is defined by the position of the emitting fluorophore and the pump stripe exit aperture. The quantity $\Omega(x, z)/2\pi$ represents the fraction of spontaneous emission propagating along the pump stripe to the exit aperture. For increasing separation between the local fluorescence emission and the sample edge, the effective fluorescence density converges to $I'_{\text{fl,eff}}(z) \propto z^{-1}$. The fact that the coupling efficiency to the fiber depends on the position of the fluorophore to the end facet is included in this model through the coupling efficiency factor $\gamma(x, z)$. This correction factor is influenced by the numerical aperture and core diameter of the fiber, and the pump stripe width. To a good approximation a geometry dependent parameter z_0 can be introduced, which accounts for all these geometrical influences. In the following, the effective fluorescence density is assumed to follow the relation

$$I'_{\text{fl,eff}}(z) \propto \frac{1}{z + z_0}. \quad (2)$$

The validity of Eq. (2) as a suitable model for a fiber-coupled pump stripe geometry was verified through numerical calculations and confirmed by measurement data.

In the presence of gain the change of light intensity I_{ASE} along the pump stripe in a slab

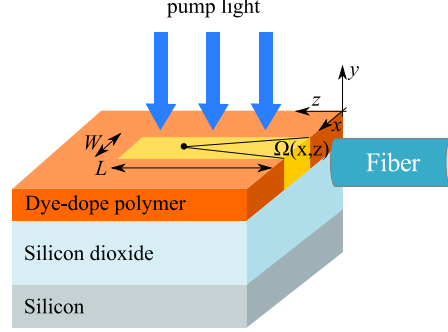


Fig. 4. Schematic drawing of the fiber-coupled variable stripe length (VSL) method to measure modal gain. The pump stripe has a length L and width W . The solid angle of the fluorescence emission at position (x, z) subtended by the pump stripe output facet is denoted with $\Omega(x, z)$.

waveguide thin film system can be written as differential equation (cf. [29, 40]) of the form

$$\frac{dI_{\text{ASE}}}{dz} = g_{\text{mod}} I_{\text{ASE}} + I'_{\text{fl,eff}}(z). \quad (3)$$

The solution of the differential equation with the emission coupling model in Eq. (2) and satisfying the boundary condition $I_{\text{ASE}}(0) = 0$, results in

$$I_{\text{ASE}}(L) = A \exp(g_{\text{mod}}(L + z_0)) [\text{Ei}(-g_{\text{mod}}(L + z_0)) - \text{Ei}(-g_{\text{mod}} z_0)], \quad (4)$$

where Ei denotes the *exponential integral* defined as

$$\text{Ei}(z) = \int_{-z}^{\infty} \frac{\exp(-t)}{t} dt. \quad (5)$$

The coefficient A in Eq. (4) is a fluorescence intensity coefficient. Without taking the correction term $\Omega(x, z)\gamma(x, z)/2\pi$ into account, the amount of fluorescence light contributing to I_{ASE} would be overestimated. As a consequence, g_{mod} derived from the measured VSL data would be underestimated. This becomes particularly apparent for low dye concentrations, where high negative gain would be derived from the data.

In the limit of a long pump stripe the solid angle $\Omega(x, z)$ can be assumed constant. The fraction of spontaneous emission contributing to ASE results in $\Omega/2\pi \approx W/L$. If the coupling to the light collecting optics is independent of the pump stripe output emission angle, the coupling efficiency γ is constant. In summary, this results in the exponential dependence of the ASE intensity [29]

$$I_{\text{ASE}}(L) = \frac{A}{g_{\text{mod}}} \left(e^{g_{\text{mod}} L} - 1 \right), \quad (6)$$

as a solution of Eq. (3). Equation (6) is commonly used for optical pump setups where long pump stripes are realized and geometric effects do not influence the gain measurements [29, 30]. However, in this work the laser diode driven VSL optical setup required the use of the more general result from Eq. (4) to obtain valid gain values. For reliable gain measurements the pump stripe length should not exceed the saturation length L_{sat} of the studied system [29, 30], which is fulfilled for the maximum pump length and gain materials in this work. Exemplary VSL curves are presented in section 3, Fig. 9(a). For ASE intensities reaching the saturation level, Eq. (4) is no longer valid and has to be refined to account for saturation effects [33, 34].

The modal gain g_{mod} can be broken down into additional terms to distinguish between different contributions, such that [29]

$$g_{\text{mod}} = \Gamma g_{\text{mat}} - \alpha_{\text{mod}}, \quad (7)$$

where Γ denotes the confinement factor of the thin film mode, and α_{mod} is a loss term that includes modal losses of an undoped thin film system, e.g. surface scattering or power leakage into the substrate. In contrast, polymer material loss and dye doping dependent losses are included in the material gain expression through a material loss term α_{mat} , which yields

$$g_{\text{mat}} = g_{\text{int}} - \alpha_{\text{mat}}. \quad (8)$$

The material loss α_{mat} includes re-absorption and scattering of the fluorescence light, and g_{int} is a bulk material internal gain. Equation (7) can be rewritten as

$$g_{\text{mod}} = \Gamma g_{\text{int}} - \alpha, \quad (9)$$

where the loss α represents both material and modal losses

$$\alpha = \Gamma \alpha_{\text{mat}} + \alpha_{\text{mod}} \quad (10)$$

and is dependent on the doping level of dye molecules in the host polymer.

2.5. Concentration quenching model

Concentration quenching in a gain material is a parasitic effect that occurs when the dye concentration in the host material is increased beyond a critical value above which the average distance between dye molecules becomes so small that intermolecular interactions start to adversely affect the dye properties. Concentration quenching reduces the fluorescence quantum yield η_{QY} of the gain material and, consequently, limits the performance. In the following, we elaborate a model that allows expressing the material gain g_{mat} as a function of the dye concentration taking into account concentration quenching.

An exponential dependence of η_{QY} on the average molecular separation r between dye molecules embedded in PMMA has been observed by Green et al. [25]. Therefore, we model the fluorescence quantum yield, using the relation $r \propto N^{-1/3}$, as

$$\eta_{\text{QY}}(N) = \eta_0 \left(1 - e^{-\beta' r^{-1/3} (N^{-1/3} - N_0^{-1/3})} \right), \quad (11)$$

with the molecular densities of the dye N and N_0 , the quenching strength β' , and the low concentration, i.e. non-quenched, quantum yield constant η_0 . The parameter N_0 represents the molecular density at which the quantum yield vanishes. By definition, the quantum yield is the ratio between fluorescence lifetime τ_f and radiative lifetime τ_{rad} , namely

$$\eta_{\text{QY}}(N) = \frac{\tau_f(N)}{\tau_{\text{rad}}}, \quad (12)$$

where the radiative decay time τ_{rad} is assumed to be independent of the molecular dye density. On the other hand, the fluorescence lifetime $\tau_f(N)$ is defined as the inverse of the sum of the radiative, non-radiative, and concentration quenching decay rates k_R , k_{NR} , k_{CQ} [25]

$$\tau_f(N) = \frac{1}{k_R + k_{\text{NR}} + k_{\text{CQ}}(N)}. \quad (13)$$

Therefore, the quantum yield becomes dependent on the molecular density of the embedded dye in the host matrix through the concentration quenching decay rate. To estimate the influence

of $\eta_{QY}(N)$ on the population inversion, the steady state rate equation, neglecting intersystem crossing (ISC) or additional higher order decay paths,

$$\frac{dS_1}{dt} = \sigma_{\text{abs}} I_p S_0 - \left(\frac{1}{\tau_f} + \sigma_{\text{em}} I \right) S_1 = 0 \quad (14a)$$

$$S_0 + S_1 = 1 \quad (14b)$$

with the relative singlet state populations S_1 and S_0 , the pump photon density I_p , the emission photon density I , and the absorption cross section σ_{abs} , is solved for S_1 resulting in

$$S_1 = \frac{\tau_f \sigma_{\text{abs}} I_p}{1 + \tau_f (\sigma_{\text{em}} I + \sigma_{\text{abs}} I_p)} \approx \tau_f \sigma_{\text{abs}} I_p. \quad (15)$$

The approximation used in Eq. (15) is only valid in a small signal approximation $I \ll I_p$ and for low to moderate pump intensities where saturation effects can still be neglected such that the singlet state population S_1 depends linearly on the pump photon density. For typical values of organic dyes, which amount to $\sigma_{\text{abs}} \approx 1 \times 10^{-16} \text{ cm}^2$ and $\tau_f \approx 2 \text{ ns}$ [7], and a pump intensity of 150 kW cm^{-2} , the deviation is below 10%. At high pump intensities, saturation effects limit the relative singlet state population to $S_1 < 1$ and the approximation in Eq. (15) is no longer valid.

The internal material gain g_{int} used in Eq. (8) to express the material gain g_{mat} depends linearly on the emission cross section σ_{em} and the population inversion density ΔN between the upper and lower level of the lasing transition, such that

$$g_{\text{int}} = \sigma_{\text{em}} \Delta N. \quad (16)$$

For organic dyes the non-radiative relaxation from the lower fluorescence level to the ground state S_0 is usually a very fast decay path. This allows approximating the population inversion by $\Delta N \approx S_1 N$. Employing Eq. (12) and Eq. (15) the internal material gain can then be expressed as a function of the molecular density of the dye N , i.e.

$$g_{\text{int}}(N) \approx \sigma_{\text{em}} S_1 N = \eta_{QY}(N) \tau_{\text{rad}} \sigma_{\text{em}} \sigma_{\text{abs}} I_p N. \quad (17)$$

The internal material gain, using the quantum yield expression from Eq. (11), can be written as

$$g_{\text{int}}(N) = \eta_0 \left(1 - e^{-\beta^{-1/3} (N^{-1/3} - N_0^{-1/3})} \right) \tau_{\text{rad}} \sigma_{\text{em}} \sigma_{\text{abs}} I_p N. \quad (18)$$

Expressing the dye content in the thin film through the weight ratio

$$w \approx \frac{N \cdot M}{\rho \cdot N_A}, \quad (19)$$

with the polymer density ρ , the molar mass M of the dye, and the Avogadro constant N_A , Eq. (18) can be formulated as a function of the weight ratio of the dye

$$g_{\text{int}}(w) = K(w) I_p \quad (20)$$

with the mass fraction dependent gain efficiency

$$K(w) = w \frac{\rho \cdot N_A}{M} \eta_0 \left(1 - e^{-\beta^{-1/3} (w^{-1/3} - w_0^{-1/3})} \right) \tau_{\text{rad}} \sigma_{\text{em}} \sigma_{\text{abs}}. \quad (21)$$

The quenching strength β in Eq. (21) differs from β' in Eq. (11) by a constant factor arising out of the change from the molecular density N to the mass fraction w . Based on Eq. (20) and Eq. (9) the modal gain g_{mod} results in

$$g_{\text{mod}}(w) = \Gamma g_{\text{int}} - \alpha \quad (22a)$$

$$= \Gamma K(w) I_p - \alpha. \quad (22b)$$

Since we are investigating dye doped polymer thin films at low to moderate doping levels, the vertical reduction of the pump light from absorption is neglected and the pump photon density I_p is assumed constant inside the gain material. A spatial variation of the pump intensity leads to a local variation of gain. In particular, pump diffraction effects can cause artificial gain [29]. Special care was taken in the design of the optical setup to minimize these effects by placing the variable slit at the position of an intermediate image.

3. Results and discussion

3.1. Absorbance and emission

Absorbance and emission spectra of 2.0 wt.% PMN in PMMA and PC, and 1.0 wt.% DCM embedded in PMMA are shown in Fig. 5(a) and Fig. 5(b), respectively. The absorbance peaks of PMN and DCM are located at 440 nm and 480 nm, respectively. Efficient absorption at the laser diode pump wavelength is expected for both dyes, as the excitation wavelength of 450 nm is close to the absorbance peaks. Peak emission wavelengths for PMN and DCM are 564 nm and 578 nm, respectively. The large Stokes shifts of 124 nm for PMN and 98 nm for DCM reduce the influence of re-absorption. Only a minor red shift was observed for PMN in PC films with respect to PMN in PMMA films.

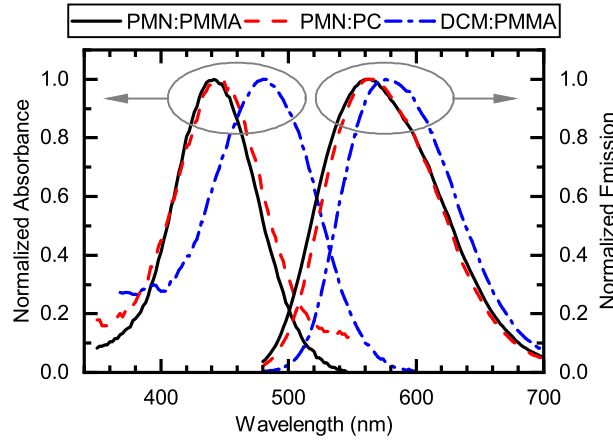


Fig. 5. Normalized absorbance and emission spectra for PMN (2.0 wt.%) in PC, and PMN (2.0 wt.%) and DCM (1.0 wt.%) in PMMA. Excitation wavelength for fluorescence emission spectra was set to 450 nm, corresponding to the operation wavelength of the pump laser diode used in gain measurements.

3.2. Material gain and concentration quenching

To obtain valid material gain data for a concentration quenching analysis, the geometrical correction described in section 2.4 had to be taken into account to accommodate the effect of the pump stripe geometry and fiber coupling efficiency present in our VSL measurement setup. In a first step, the concentration dependent loss α was determined by shifting an excitation stripe orientated parallel to the sample edge. A parallel orientation of the excitation stripe effectively reduced the influence of mode spreading and of the NA of the collecting fiber. An exponential fit to the obtained intensity data was used to extract the loss α , shown in Fig. 6(a), which was repeated for various dye concentrations of PMN and DCM in the two host polymer materials. Subsequently, the modal loss α_{mod} was derived from the intercept with the y-axis of a linear data fit to the loss α and amounted to less than 3 cm^{-1} for both PMMA and PC. Loss increased

moderately for increasing dye concentrations in PMN doped polymers, whereas a strong rise in loss was measured for DCM. The significantly higher loss of DCM compared to PMN could be a result of absorbing impurities present in the employed DCM dye and re-absorption of the fluorescence light in the emission wavelength region despite the strong Stoke's shift. In general, high loss reduces modal gain and no light amplification occurs at elevated dye concentrations. Results of the performed loss measurements are summarized in Fig. 6(b), where the linear fits to the determined losses for different dye concentrations are presented.

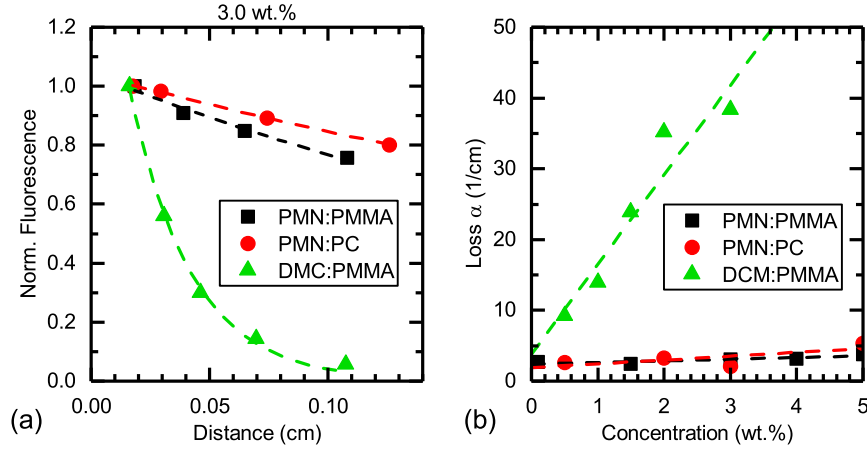


Fig. 6. (a) Dependence of fluorescence intensity on distance of excitation stripe from the sample edge. The pump stripe was orientated parallel to the sample edge to minimize the influence of the fiber NA on the measurement. Dashed lines present exponential fit to the data. (b) Derived losses $\alpha = \Gamma\alpha_{\text{mat}} + \alpha_{\text{mod}}$ from shifting excitation stripe measurements. Dashed lines present a linear fit to the loss.

The fitting parameter z_0 , which is required to model the ASE intensity using Eq. (4), was extracted from measurements at low dye concentrations (0.1 wt.%), for which ASE becomes negligible, i.e. vanishing internal gain, and spontaneous emission dominates. Subsequently, the parameter z_0 and the determined loss values were used to extract the internal gain from the VSL data at different dye concentrations of PMN and DCM in the corresponding polymer material systems. The internal gain is related to the modal gain through Eq. (9).

For PMN, a peak internal gain Γ_{gint} of $43 \pm 2 \text{ cm}^{-1}$ was obtained at a concentration of 5.0 wt.% in PMMA, whereas a peak internal gain of $35 \pm 6 \text{ cm}^{-1}$ at a concentration of 4.0 wt.% was reached in PC. The influence of concentration quenching on the internal gain was more pronounced in PC than in PMMA. For DCM in PMMA the peak internal gain of $34 \pm 3 \text{ cm}^{-1}$ occurred at a significantly lower concentration of 1.5 wt.%. Figures 7(a) and 7(b) summarize the internal gain Γ_{gint} characteristics of both PMN and DCM, including best fits to Eq. (20) on the measured gain. The obtained quenching parameters are summarized in Table 1.

Table 1. Concentration quenching parameters derived from gain measurements.

Dye	Polymer	w_0 (wt.%)	$\beta^{-1/3}$ (wt.% ^{1/3})
PMN	PMMA	11 ± 2	4 ± 2
PMN	PC	6.0 ± 0.5	17 ± 7
DCM	PMMA	3.4 ± 0.1	2 ± 1

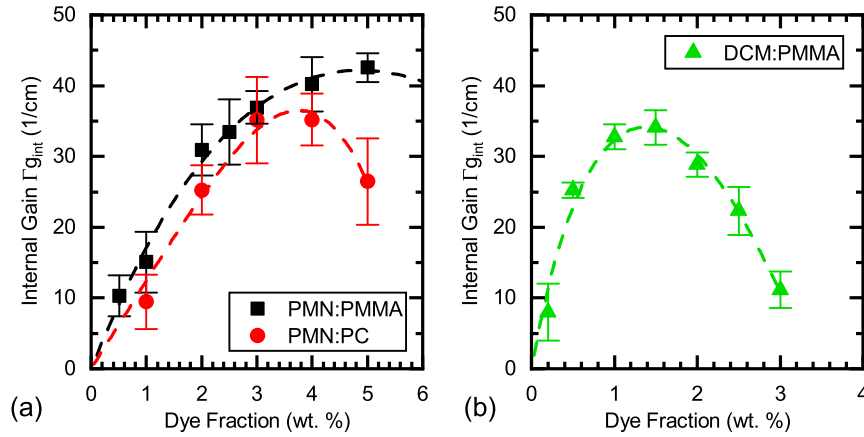


Fig. 7. Dependence of internal material gain g_{int} on dye mass fraction for different dye-doped thin film polymers: (a) PMN:PMMA, PMN:PC, (b) DCM:PMMA. Measurements were carried out at 150 kW cm^{-2} pump intensity and 35 ns pulse width. Graphs include best fits to the proposed concentration quenching gain model, shown as dashed lines.

The quenching concentration w_0 , which describes the dye concentration for which the internal gain ultimately vanishes due to dye molecule intermolecular interaction, was highest for PMN in PMMA with (11 ± 2) wt.%, suggesting a good performance at high concentrations. Concentration quenching set in at lower concentrations in the PC host polymer, with a model parameter w_0 of (6.0 ± 0.5) wt.%. The quenching concentration of DCM molecule in PMMA was calculated to be (3.4 ± 0.1) wt.%. The bulky tert-butyl groups of PMN therefore not only improve the solubility of the molecule but additionally reduce dye aggregation and concentration quenching. All measured systems are well described by the proposed concentration quenching model.

While the internal gain $\Gamma_{g_{int}}$ describes the underlying quenching phenomena, modal gain includes inherent losses and is therefore an important figure to describe the net gain of the studied thin film system. A peak modal gain of 39 cm^{-1} was reached for PMN embedded in PMMA at a dye concentration of 5.0 wt.%, whereas 32 cm^{-1} was obtained for the PC host polymer at 3.0 wt.%. A peak modal gain of 16 cm^{-1} was determined for 1.0 wt.% DCM embedded in PMMA. Above 2.0 wt.%, no positive modal gain could be reached since quenching reduced the internal gain below the loss α .

In contrast to our findings, a modal gain of up to 40 cm^{-1} was reported for concentrations of DCM as high as 5.0 wt.% by Gozhyk et al. [31]. The difference can most likely be attributed to the high loss present in the tested DCM samples. Moreover, optical pumping was performed at a pulse width of 500 ps compared to 35 ns in our experiments. Such a short high intensity pulse width leads to an increased population inversion, which potentially reduces losses induced from higher order decay paths such as non-radiative intrinsic decay, intersystem crossing (ISC) to the triplet state, or molecule-molecule interaction based on Förster energy transfer. The temporal shape of the optical excitation has a significant influence on the determined gain and a direct comparison of gain values between different pump sources is in general difficult [16]. Additionally, DCM is quite sensitive to intermolecular interaction, such that typical dye concentrations do not exceed 2.0 wt.%. To overcome this limitation, Vembris et al. added bulky trityloxyethyl groups to the molecule and successfully impeded quenching for these DCM derivatives [41].

To further verify the validity of our proposed concentration quenching gain model we applied it to gain data of a DCM doped polystyrene (PS) thin film system reported by Lu et al. [38]. The modal gain values of DCM:PS films have been obtained by Lu et al. employing a Q-switched

solid-state Nd:YAG laser working at a wavelength of 532 nm. The pulse width was 8 ns at a repetition rate of 10 Hz. The loss amounted to 9.25 cm^{-1} for a concentration of 1.4 wt.%. On the basis of this values, we estimated the dye concentration dependent loss α using the linear model

$$\alpha(w) = w \frac{9.25 \text{ cm}^{-1}}{1.4 \text{ wt.}\%}, \quad (23)$$

where the contribution of the modal loss α_{mod} was neglected. Figure 8 shows the reported modal gain values of DCM in PS including a best fit to the quenching model and the derived quenching model parameters $\beta^{-1/3}$ and w_0 . The high quenching concentration of 40 wt.% suggests a good performance of DCM in the PS host matrix. However, the high losses of DCM reduce the attainable modal gain. An extrapolation of the fit indicates that the net gain vanishes beyond a concentration of 6 wt.%. Overall, the modal gain of DCM in PS is well described by the concentration quenching model.

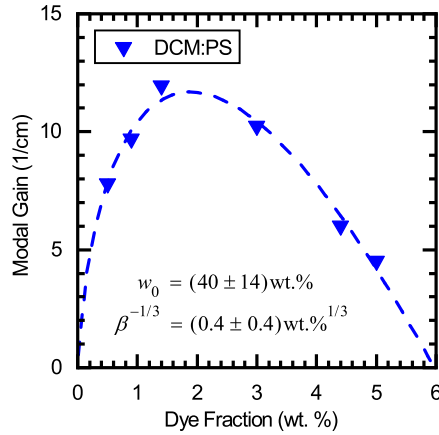


Fig. 8. Dependence of modal g_{mod} on doping concentration of DCM embedded in polystyrene (PS). Modal gain data were taken from the work of Lu et al. [38]. Excitation was performed at a wavelength of 532 nm and a pulse width of 8 ns. The dashed line represents the best fit of the proposed concentration quenching gain model. Adapted with permission from [38], *The Optical Society* (OSA).

3.3. Gain efficiency of DCM

Knowledge about the gain efficiency ΓK facilitates the design of organic solid-state lasers, as the minimum pump intensity required for lasing can be estimated from the threshold gain of the laser cavity. For a better physical insight we determined the gain efficiency of DCM experimentally and compared it to both the commonly employed linear model and to the quenched model introduced in section 2.5. For DCM the required material parameter values are well studied and available in literature.

VSL measurements were used to experimentally investigate the dependence of the internal gain Γg_{int} on the pump intensity. The gain efficiency ΓK was extracted from the slope of a linear fit to the pump intensity dependent internal gain Γg_{int} in Eq. (17). The measured VSL data and the deduced gain values for 1.0 wt.% DCM in PMMA are summarized in Figs. 9(a) and 9(b), respectively. A gain efficiency ΓK of $240 \text{ cm}^{-1} \text{ MW}^{-1}$ was determined.

The gain efficiency ΓK can also be estimated purely from material parameters. If concentration

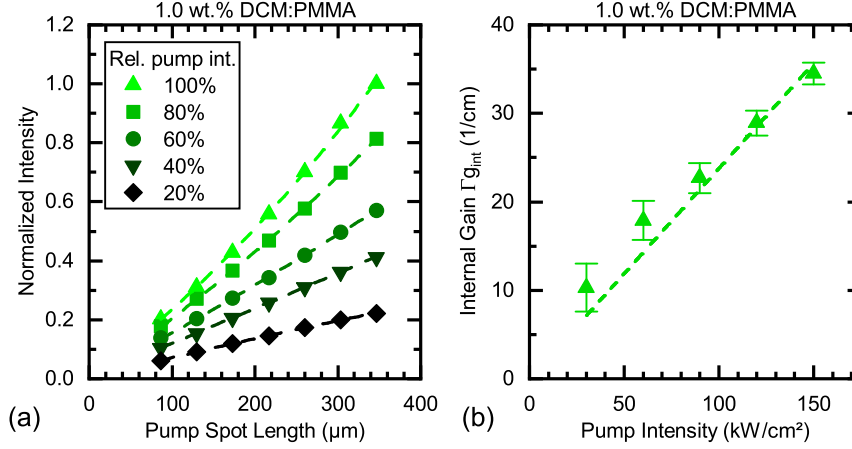


Fig. 9. (a) Normalized ASE intensity obtained from VSL gain measurements of 1.0 wt.% DCM in PMMA for different pump intensities relative to 150 kW cm^{-2} at 35 ns pulse width. (b) Dependence of internal gain $\Gamma_{g_{int}}$ on the pump intensity. The slope of a linear fit to the measured data yields the gain efficiency ΓK .

quenching is omitted, the gain efficiency can be approximated by [31]

$$K = \sigma_{em} \sigma_{abs} N \frac{\tau_f}{h\nu}, \quad (24)$$

where h represents Planck's constant and ν the pump light frequency. In the following, we calculated the theoretical modal gain efficiency for DCM in PMMA, for which the required material parameter values are well studied and available in literature. The absorption and emission cross sections of DCM in PMMA at a wavelength of 450 nm and 600 nm are $130 \times 10^{-18} \text{ cm}^2$ and $320 \times 10^{-18} \text{ cm}^2$, respectively [7]. The fluorescence decay time τ_f of DCM in PMMA is approximately 2 ns [25, 31]. The confinement factor Γ can be readily derived from eigenmode calculations, for which we used the polymer refractive index and neglected the doping contribution, resulting in a confinement factor for the TE-like polarization of approximately $\Gamma = 0.8$. In summary, a 1.0 wt.% DCM doped PMMA thin film results in a theoretical modal gain efficiency of $\Gamma K = 3500 \text{ cm}^{-1} \text{ MW}^{-1}$. These calculations significantly overestimate the gain efficiency compared to the experimentally determined value.

If we apply Eq. (21) of our gain model, which takes concentration quenching into account, the gain efficiency amounts to $\Gamma K = 417 \text{ cm}^{-1} \text{ MW}^{-1}$. In this calculation, we used the experimentally determined quenching coefficients for DCM doped PMMA summarized in Table 1. The values of the radiative lifetime $\tau_{rad} = 7.1 \text{ ns}$ and the quantum yield $\eta_0 = 0.33$ are taken from Green et al. [25]. The proposed quenching model strongly reduces the discrepancy between theory and measured data. This indicates that the linear model for the dependence of the gain efficiency on the dye concentration is only valid for low dye concentrations at which concentration quenching is negligible. For increased dye concentrations and close to the material gain peak value, quenching phenomena need to be included in the description of the system.

4. Conclusion and outlook

In this paper we present a material gain model for organic dye-doped polymers that is able to describe concentration quenching. This model was applied to measurement results of the novel organic dye molecule PMN and the reference dye DCM. For both dyes concentration quenching was well described and model parameters have been extracted. Additionally, the

presented gain model reduces the overestimation of the gain efficiency compared to a linear model, where intermolecular interaction is not included. Modal gain values were obtained by a refined VSL method. This method accounted for geometric effects arising from the narrow pump stripe and the numerical aperture of the light collecting fiber. Our results show that high power laser diodes can be used as pump light source for gain measurements in organic dye-doped polymer thin films using the VSL method. For PMN we reached a material internal gain $\Gamma_{g_{int}}$ up to 43 cm^{-1} in PMMA at a dye concentration of 5.0 wt.%, whereas for DCM we reached 34 cm^{-1} at a dye concentration of 1.5 wt.%. Taking losses into account, modal gain of 39 cm^{-1} for PMN and 16 cm^{-1} for DCM were obtained. The high achievable gain and reduced concentration quenching compared to DCM make PMN a promising organic solid-state laser dye candidate. The influence of the polymer matrix on gain properties has been investigated for PMN. Even though modal gain was reduced to 32 cm^{-1} in PC, the higher refractive index could be an interesting material property for photonic integrated circuit designs.

In a next step, the material gain model will be applied to a wider range of dyes and polymers. Moreover, future work will also address the influence of the pump intensity and the duration of the excitation pulse on concentration quenching. Furthermore, laser dye parameters such as photostability and threshold will be investigated. Ultimately, we envisage the development of a laser diode pumped integrated organic solid-state laser based on the novel dye molecule.

Funding

Austrian Research Promotion Agency (FFG) (850649).

Acknowledgments

This research has received funding through the grant PASSION (No. 850649) from the Austrian Research Promotion Agency (FFG). The authors wish to thank *ams AG* for supplying high quality silicon substrates.

References

1. H. Ma, A.-Y. Jen, and L. R. Dalton, "Polymer-based optical waveguides: Materials, processing, and devices," *Adv. Mater.* **14**, 1339–1365 (2002).
2. L. Wang, J. Ren, X. Han, T. Claes, X. Jian, P. Bienstman, R. Baets, M. Zhao, and G. Morthier, "A label-free optical biosensor built on a low-cost polymer platform," *IEEE Photonics J.* **4**, 920–930 (2012).
3. K. J. Kim, H.-J. Lee, J.-H. Lee, H.-I. Jung, J.-G. Yook, and S.-G. Kim, "A highly sensitive and label free biosensing platform for wireless sensor node system," *Biosens. Bioelectron.* **50**, 362–367 (2013).
4. O. Ostroverkhova, ed., *Handbook of Organic Materials for Optical and (Opto)Electronic Devices: Properties and Applications*, (Woodhead Publishing, Oxford, 2013).
5. A. C. Mayer, S. R. Scully, B. E. Hardin, M. W. Rowell, and M. D. McGehee, "Polymer-based solar cells," *Mater. Today* **10**, 28–33 (2007).
6. S. Günes, H. Neugebauer, and N. S. Sariciftci, "Conjugated polymer-based organic solar cells," *Chem. Rev.* **107**, 1324–1338 (2007).
7. S. Forget and S. Chénais, *Organic Solid-State Lasers*, vol. 175 of *Springer Series in Optical Sciences*, 0342-4111 (Springer Berlin Heidelberg, 2013).
8. C. W. Tang, S. A. VanSlyke, and C. H. Chen, "Electroluminescence of doped organic thin films," *J. Appl. Phys.* **65**, 3610–3616 (1989).
9. H. Nakanotani, T. Higuchi, T. Furukawa, K. Masui, K. Morimoto, M. Numata, H. Tanaka, Y. Sagara, T. Yasuda, and C. Adachi, "High-efficiency organic light-emitting diodes with fluorescent emitters," *Nat. Commun.* **5**, 4016 (2014).
10. C. Sekine, Y. Tsubata, T. Yamada, M. Kitano, and S. Doi, "Recent progress of high performance polymer OLED and OPV materials for organic printed electronics," *Sci. Technol. Adv. Mater.* **15**, 034203 (2014).
11. A. Costela, I. García-Moreno, and R. Sastre, "Polymeric solid-state dye lasers: Recent developments," *Phys. Chem. Chem. Phys.* : PCCP **5**, 4745–4763 (2003).
12. I. D. Samuel and G. A. Turnbull, "Polymer lasers: Recent advances," *Mater. Today* **7**, 28–35 (2004).
13. Y. Yang, G. A. Turnbull, and I. D. W. Samuel, "Hybrid optoelectronics: A polymer laser pumped by a nitride light-emitting diode," *Appl. Phys. Lett.* **92**, 163306 (2008).
14. C. Foucher, B. Guilhabert, J. Herrnsdorf, N. Laurand, and M. D. Dawson, "Diode-pumped, mechanically-flexible polymer DFB laser encapsulated by glass membranes," *Opt. Express* **22**, 24160–24168 (2014).

15. Z. Zhao, O. Mhibik, M. Nafa, S. Chénais, and S. Forget, "High brightness diode-pumped organic solid-state laser," *Appl. Phys. Lett.* **106**, 051112 (2015).
16. J. Herrnsdorf, Y. Wang, McKendry, Jonathan J. D., Z. Gong, D. Massoubre, B. Guilhabert, G. Tsiminis, G. A. Turnbull, Samuel, Ifor D. W., N. Laurand, E. Gu, and M. D. Dawson, "Micro-led pumped polymer laser: A discussion of future pump sources for organic lasers," *Laser & Photonics Rev.* **7**, 1065–1078 (2013).
17. A. J. C. Kuehne and M. C. Gather, "Organic lasers: Recent developments on materials, device geometries, and fabrication techniques," *Chem. Rev.* **116**, 12823–12864 (2016).
18. D. Beer and J. Weber, "Photobleaching of organic laser dyes," *Opt. Commun.* **5**, 307–309 (1972).
19. E. McKenna, J. Xue, A. Verdoni, M. Yetzbacher, R. Fan, and A. Mickelson, "Kinetic model of irreversible photobleaching of dye-doped polymer waveguide materials," *J. Opt. Soc. Am. B* **21**, 1294 (2004).
20. P. P. Mondal, "Minimizing photobleaching in fluorescence microscopy by depleting triplet states," *Appl. Phys. Lett.* **92**, 013902 (2008).
21. P. Bollgruen, U. Gleissner, T. Wolfer, C. Megnin, D. Mager, L. Overmeyer, J. G. Korvink, and T. Hanemann, "Ink-jet printed fluorescent materials as light sources for planar optical waveguides on polymer foils," *Opt. Eng.* **55**, 107107 (2016).
22. J. Alamán, R. Alicante, J. Peña, and C. Sánchez-Somolinos, "Inkjet printing of functional materials for optical and photonic applications," *Materials* **9**, 910 (2016).
23. I. Wieder, "Quenching of laser dye fluorescence by absorption from an excited singlet state," *Appl. Phys. Lett.* **21**, 318–320 (1972).
24. S. Speiser, R. van der Werf, and J. Kommandeur, "Photoquenching: The dependence of the primary quantum yield of a monophotonic laser-induced photochemical process on the intensity and duration of the exciting pulse," *Chem. Phys.* **1**, 297–305 (1973).
25. A. P. Green and A. R. Buckley, "Solid state concentration quenching of organic fluorophores in PMMA," *Phys. Chem. Chem. Phys.* **17**, 1435–1440 (2015).
26. M. Amyot-Bourgeois, E. K. Keshmarzi, C. Hahn, R. N. Tait, and P. Berini, "Gain optimization, bleaching, and e-beam structuring of IR-140 doped PMMA and integration with plasmonic waveguides," *Opt. Mater. Express* **7**, 3963 (2017).
27. R. Muñoz-Mármol, N. Zink-Lorre, J. M. Villalvilla, P. G. Boj, J. A. Quintana, C. Vázquez, A. Anderson, M. J. Gordon, A. Sastre-Santos, F. Fernández-Lázaro, and M. A. Díaz-García, "Influence of blending ratio and polymer matrix on the lasing properties of perylenediimide dyes," *The J. Phys. Chem. C* **122**, 24896–24906 (2018).
28. K. L. Shaklee and R. F. Leheny, "Direct determination of optical gain in semiconductor crystals," *Appl. Phys. Lett.* **18**, 475–477 (1971).
29. L. Negro, P. Bettotti, M. Cazzanelli, D. Pacifici, and L. Pavesi, "Applicability conditions and experimental analysis of the variable stripe length method for gain measurements," *Opt. Commun.* **229**, 337–348 (2004).
30. L. Cerdán, A. Costela, and I. García-Moreno, "On the characteristic lengths in the variable stripe length method for optical gain measurements," *J. Opt. Soc. Am. B* **27**, 1874 (2010).
31. I. Gozhyk, M. Boudreau, H. R. Haghighi, N. Djellali, S. Forget, S. Chénais, C. Ulysse, A. Brosseau, R. Pansu, J.-F. Audibert, S. Gauvin, J. Zyss, and M. Lebental, "Gain properties of dye-doped polymer thin films," *Phys. Rev. B* **92**, 214202 (2015).
32. S. Bäumer, *Handbook of Plastic Optics* (Wiley-VCH Verlag GmbH & Co. KGaA, Weinheim, Germany, 2010).
33. A. Costela, O. García, L. Cerdán, I. García-Moreno, and R. Sastre, "Amplified spontaneous emission and optical gain measurements from pyromethene 567-doped polymer waveguides and quasi-waveguides," *Opt. Express* **16**, 7023 (2008).
34. A. Costela, O. García, L. Cerdán, I. García-Moreno, and R. Sastre, "Amplified spontaneous emission and optical gain measurements from pyromethene 567-doped polymer waveguides and quasi-waveguides: erratum," *Opt. Express* **16**, 7587 (2008).
35. J. S. Klimavicz, J. F. Mike, A. Bhuwarka, A. L. Tomlinson, and M. Jeffries-EL, "Synthesis of benzobisoxazole-based D- π -A- π -D organic chromophores with variable optical and electronic properties," *Pure Appl. Chem.* **84**, 991–1004 (2012).
36. E. Ishow, A. Brosseau, G. Clavier, K. Nakatani, P. Tauc, C. Fiorini-Debuisschert, S. Neveu, O. Sandre, and A. Léaustic, "Multicolor emission of small molecule-based amorphous thin films and nanoparticles with a single excitation wavelength," *Chem. Mater.* **20**, 6597–6599 (2008).
37. H. Rabbani-Haghighi, S. Forget, S. Chénais, A. Siove, M.-C. Castex, and E. Ishow, "Laser operation in nondoped thin films made of a small-molecule organic red-emitter," *Appl. Phys. Lett.* **95**, 033305 (2009).
38. W. Lu, B. Zhong, and D. Ma, "Amplified spontaneous emission and gain from optically pumped films of dye-doped polymers," *Appl. Opt.* **43**, 5074 (2004).
39. I. Gozhyk, G. Clavier, R. Méallet-Renault, M. Dvorko, R. Pansu, J.-F. Audibert, A. Brosseau, C. Lafargue, V. Tsvirkun, S. Lozenko, S. Forget, S. Chénais, C. Ulysse, J. Zyss, and M. Lebental, "Polarization properties of solid-state organic lasers," *Phys. Rev. A* **86** (2012).
40. P. W. Milonni and J. H. Eberly, *Laser Physics* (Wiley-Blackwell, Oxford, 2010).
41. A. Vembris, E. Zarins, and V. Kokars, "Stimulated emission and optical properties of pyranilyden fragment containing compounds in PVK matrix," *Opt. & Laser Technol.* **95**, 74–80 (2017).